



Delft University of Technology

## Mudflat Morphodynamics and the Impact of Sea Level Rise in South San Francisco Bay

van der Wegen, Mick; Jaffe, Bruce; Foxgrover, Amy; Roelvink, Dano

**DOI**

[10.1007/s12237-016-0129-6](https://doi.org/10.1007/s12237-016-0129-6)

**Publication date**

2016

**Document Version**

Final published version

**Published in**

Estuaries and Coasts

**Citation (APA)**

van der Wegen, M., Jaffe, B., Foxgrover, A., & Roelvink, D. (2016). Mudflat Morphodynamics and the Impact of Sea Level Rise in South San Francisco Bay. *Estuaries and Coasts*, 40(1), 37-49.  
<https://doi.org/10.1007/s12237-016-0129-6>

**Important note**

To cite this publication, please use the final published version (if applicable).  
Please check the document version above.


**Copyright**

Other than for strictly personal use, it is not permitted to download, forward or distribute the text or part of it, without the consent of the author(s) and/or copyright holder(s), unless the work is under an open content license such as Creative Commons.

**Takedown policy**

Please contact us and provide details if you believe this document breaches copyrights.  
We will remove access to the work immediately and investigate your claim.

# Mudflat Morphodynamics and the Impact of Sea Level Rise in South San Francisco Bay

Mick van der Wegen<sup>1,2</sup>  • Bruce Jaffe<sup>3</sup> • Amy Foxgrover<sup>3</sup> • Dano Roelvink<sup>1,2,4</sup>

Received: 19 January 2016 / Revised: 23 May 2016 / Accepted: 18 June 2016 / Published online: 12 August 2016  
© The Author(s) 2016. This article is published with open access at Springerlink.com

**Abstract** Estuarine tidal mudflats form unique habitats and maintain valuable ecosystems. Historic measurements of a mudflat in San Francisco Bay over the past 150 years suggest the development of a rather stable mudflat profile. This raises questions on its origin and governing processes as well as on the mudflats' fate under scenarios of sea level rise and decreasing sediment supply. We developed a 1D morphodynamic profile model (Delft3D) that is able to reproduce the 2011 measured mudflat profile. The main, schematised, forcings of the model are a constant tidal cycle and constant wave action. The model shows that wave action suspends sediment that is transported landward during flood. A depositional front moves landward until landward bed levels are high enough to carry an equal amount of sediment back during ebb. This implies that, similar to observations, the critical shear stress for erosion is regularly exceeded during the tidal cycle and that modelled

equilibrium conditions include high suspended sediment concentrations at the mudflat. Shear stresses are highest during low water, while shear stresses are lower than critical (and highest at the landward end) along the mudflat during high water. Scenarios of sea level rise and decreasing sediment supply drown the mudflat. In addition, the mudflat becomes more prone to channel incision because landward accumulation is hampered. This research suggests that sea level rise is a serious threat to the presence of many estuarine intertidal mudflats, adjacent salt marshes and their associated ecological values.

**Keywords** Mudflat · Equilibrium · Morphodynamic modelling · Sea level rise · San Francisco Bay

Communicated by Marianne Holmer

**Key points** We reproduce a measured mudflat profile in equilibrium with a 1D morphodynamic model  
Equilibrium conditions pertain high SSC levels on the mudflat  
Mudflats drown and become less stable under scenarios of sea level rise and decreasing sediment supply.

**Electronic supplementary material** The online version of this article (doi:10.1007/s12237-016-0129-6) contains supplementary material, which is available to authorized users.

✉ Mick van der Wegen  
m.vanderwegen@unesco-ihe.org

## Introduction

### Framework

Estuarine tidal mudflats form unique and valuable habitat areas, which are flooded and become exposed again during a tidal cycle. Amongst other ecological values, mudflats accommodate microphytobenthos (e.g. diatoms) and serve as feeding ground for (migratory) birds and fish (e.g. Herman et al. 1999). In addition, mudflats provide important sources of sediment for adjacent salt marshes (e.g. Van Wijnen et al. 2001; Temmerman et al. 2004; Ganju et al. 2015). As such, mudflats are an integral part of the estuarine coastline and play an important role in flood defence (e.g. Möller et al. 2014).

The mudflat shape and elevation are correlated to prevailing conditions of wind waves and tides (Bearman et al. 2010), while sediment availability and biotic dynamics play an important (seasonal) role as well. Mudflats will adapt to sea level rise and gradually changing sediment supply on a much longer timescale (~decades) (Le Hir et al. 2000; Friedrichs 2012).

<sup>1</sup> UNESCO-IHE, PO Box 3015, 2601 DA Delft, The Netherlands

<sup>2</sup> Deltares, PO Box 177, 2601 DA Delft, The Netherlands

<sup>3</sup> USGS, Pacific Coastal and Marine Science Center, 400 Natural Bridges Drive, Santa Cruz, CA 95060, USA

<sup>4</sup> CITG TU Delft, PO Box 5048, 2600 GA Delft, The Netherlands

Several model attempts have been made to further understand mudflat morphodynamics. Friedrichs and Aubrey (1996) derived analytical equilibrium profiles assuming no spatial gradients in bed shear stress by the action of either waves or tides. The forcing determined the shape of their solutions so that tidal forcing led to more convex and wave forcing to more concave solutions. Including evolution of the mudflat profile by an adaptation timescale, Hu et al. (2015) allowed morphodynamic adaptations toward equilibrium conditions based on the criterion of a uniform bed shear stress across the mudflat profile.

Others followed a fully process-based approach which included a detailed process description of hydrodynamics, sediment transport and eventually bed level updates without underlying assumptions on equilibrium conditions. Hsu et al. (2013) and Van Maren and Winterwerp (2013) explored the suspended sediment dynamics on a fixed bed. By including a morphodynamic feedback, Pritchard et al. (2002) and Pritchard and Hogg (2003) confirmed the (tide forced only) equilibrium profiles by Friedrichs and Aubrey (1996). More recently, Maan et al. (2015) suggested the possibility that mudflats under cross-shore tidal forcing, either prograde or retreat while maintaining a migrating, several kilometres long, equilibrium profile shape. Zhou et al. (2015a, 2016) explored the impact of grain sorting and consolidation on mudflat morphodynamics, while Marani et al. (2007), Mariotti and Fagherazzi (2010) and Zhou et al. (2015b) provide examples on the impact of vegetation and its feedback on morphodynamics.

Considering a realistic case study, Roberts et al. (2000) validated a morphodynamic model against a 3 km long observed mudflat profile in the Humber estuary with a bias of about 50 cm. Roberts et al. (2000) thus showed that the process-based approach could reach an equilibrium mudflat profile using the prevailing tide and schematised wave conditions. Remarkably, relatively high suspended sediment concentrations were present on the mudflat which could be related to subsequent periods of erosion and deposition during the tidal cycle. Still, after profile equilibrium was reached, there was no tide-residual morphodynamic effect. This confirms findings by Hu et al. (2015).

In addition to schematised profile modelling, Van der Wegen et al. (2011), Van der Wegen and Jaffe (2013), Ganju et al. (2009), and Ganju and Schoellhamer (2010) reported skillful, decadal timescale, hindcasts of morphodynamic mudflat development in sub-embayments of San Francisco Bay by 2DH process-based models. Van der Wegen and Jaffe (2014) further analysed the detailed (tidal timescale) underlying processes and concluded that significant morphodynamic activity took place during a tidal cycle, while tide-residual morphological developments were an order of magnitude smaller. In their model, Van der Wegen and Jaffe (2014) further observed that deposition and erosion of the channel-shoal interface occurred during both ebb and flood. A more governing condition for net deposition appeared to be high suspended sediment

concentration caused by river supply or wind waves suspending sediments from the mudflat.

The previous sections indicate that considerable sensitivity analysis was carried out on important parameters in mudflat development and assumed profile equilibrium conditions. Some studies were able to reproduce measured profiles with significant skill. As a next step, it is important to address the adaptation of mudflats to changing forcing conditions.

The objective of this work is to assess the conditions of mudflat equilibrium as well as the impact of sediment supply and sea level rise on mudflat evolution. Our inspiration is the mudflat near Dumbarton Bridge in South San Francisco Bay, which has a detailed and historic bathymetric dataset available for model calibration and validation.

## Methodology

We use a combination of observations and 1D process-based modelling (Delft3D). Close analysis of a series of bathymetric surveys collected approximately every 30 years from 1858 to 2005 will describe the historic evolution of Dumbarton mudflat and will help to hypothesise on the mechanisms governing the mudflat evolution.

The aim of the modelling work is to reproduce the current mudflat profile while exploring conditions of equilibrium. This includes extensive sensitivity analysis on model input parameters related to sediment characteristics, wind wave forcing and tidal dynamics. Finally, starting from a generated equilibrium profile, we assess the impact of sea level rise and a decay in sediment supply on profile development. These predictions will provide insight into the future development of the mudflat and its value for ecology and flood protection.

## Study Area

### Physical Setting

Situated within the largest estuary on the west coast of the USA, South San Francisco Bay is a relatively shallow sub-estuary in the San Francisco Estuary with an average depth of approximately 3 m and a surface area of about 400 km<sup>2</sup> (Fig. 1, Foxgrover et al. 2004). The bathymetry of South San Francisco Bay is simple with a single main channel flanked by broad shallows and intertidal flats (Fig. 1). The channel narrows from about 1 km in the north to several hundred meters in the south. The channel also shoals from north to south from approximately 25- to 5-m depth.

Water movement in South San Francisco Bay is driven by tides, winds and freshwater flow from seasonal streams (Conomos and Peterson 1977; Walters et al. 1985; Cheng et al. 1993). San Francisco Bay experiences a Mediterranean climate with cool wet winters and relatively dry summers accompanied by persistent northerly to northwesterly winds.

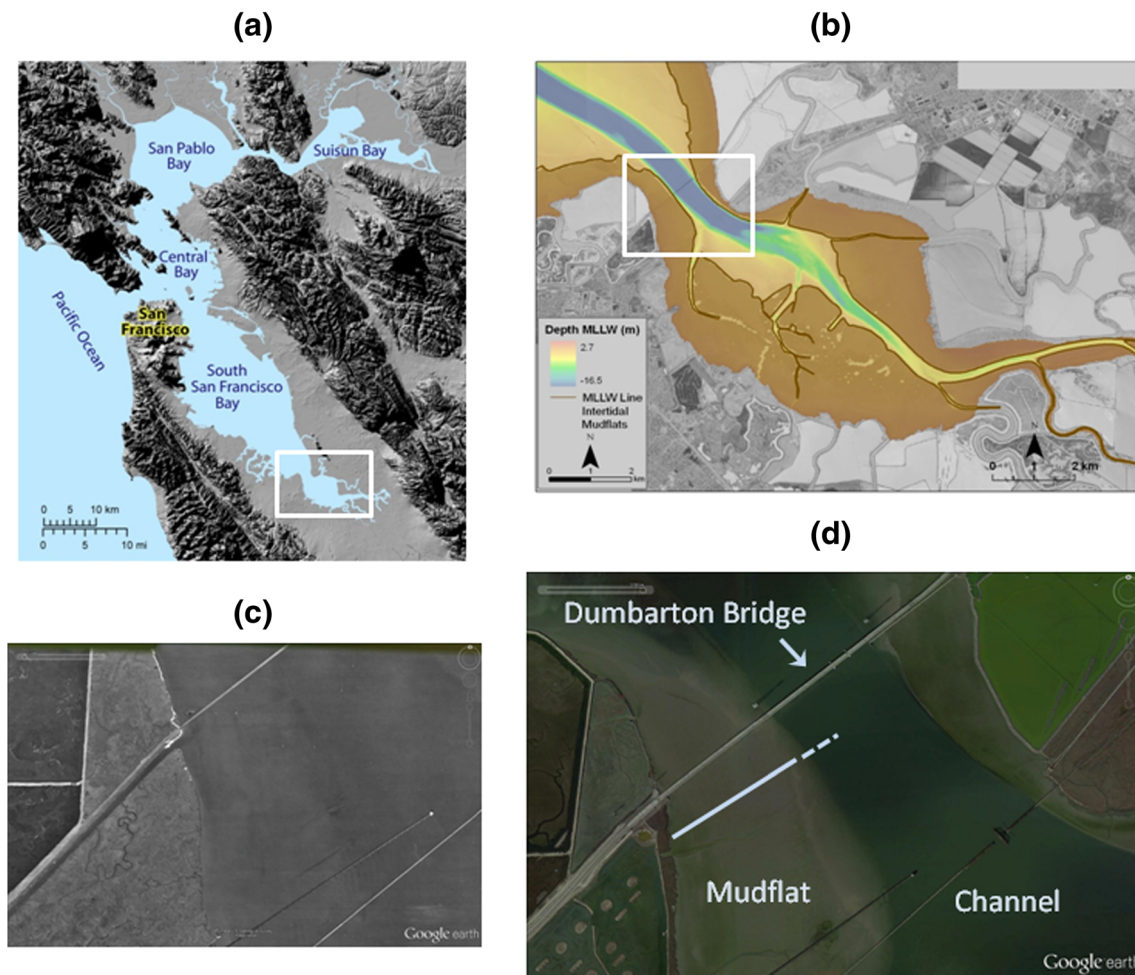


**Fig. 1** Location of Dumbarton mudflat **a** in San Francisco Bay and **b** in South Bay, **c** in 1948 and **d** in 2012. Line in **d** reflects transect analysed in this study, with *dashed part* being the channel. **c**, **d** are from Google Earth

Wind-driven waves resulting from these persistent winds play a strong role in intertidal sediment transport (Lacy et al. 1996, 2014). During the winter, frequent storms (cyclonic low-pressure atmospheric systems) transit the region and cause strong, gusty southerly to southeasterly winds. These storms often bring substantial rainfall to local land areas with subsequent runoff into the bay (Conomos et al. 1985). Local streams and small creeks that enter South San Francisco Bay discharge varying amounts of sediment and freshwater during and after flooding (Schoellhamer 1996). Winter runoff into North San Francisco Bay and Delta from the Sacramento and San Joaquin River systems influences water levels and flows in South San Francisco Bay. However, the exchange of water between North and South San Francisco Bays, and the effects of this exchange on circulation and sediment transport are not well understood (Walters et al. 1985).

#### *Intertidal Mudflat Characteristics and History*

Intertidal flats are a major component of South San Francisco Bay. In 2005, intertidal flat area was  $51.2 \pm 4.8/-5.8 \text{ km}^2$

(Jaffe and Foxgrover 2006). The asymmetry in the error is caused by positional error acting on different slopes. Nearly half of the intertidal flats were in the low energy, higher tidal range environment south of Dumbarton Bridge. Intertidal flat width increases from north to south from 200 to 900 m. The surface sediments within South San Francisco Bay are primarily composed of silts with a mean grain size of approximately  $50 \mu$ . The vast majority of samples are greater than 75 % mud, although some coarser sediments with higher sand and shell contents are found on the eastern shoals (Barnard et al. 2013; Jones and Jaffe 2013).

The specific area in South San Francisco Bay, the western shore south of Dumbarton Bridge, where the proposed model is tested, is dynamic at various time scales. The current tidal flat elevation varies from about  $-2$  to  $0 \text{ MSL}$ . The mudflat width is correlated with net deposition/erosion patterns in the entire South Bay. In historic times, the tidal flats have widened by a factor of two during decadal periods of net sediment import and narrowed during net sediment export from South Bay (Fig. 2). Bearman et al. (2010) suggest that the mudflats in the area around Dumbarton Bridge have been fairly stable

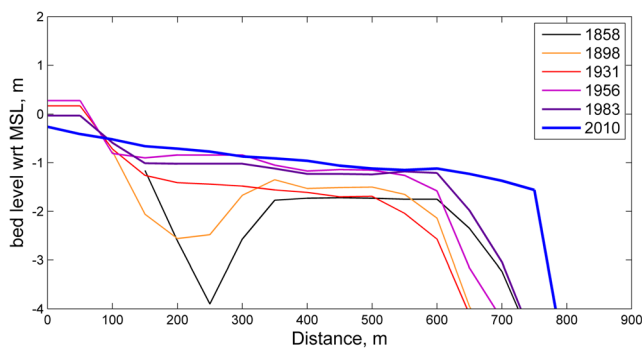


**Fig. 2** Historical profiles along transect of Fig. 1d

between 1983 and 2005 without much net profile change. Still, seasonal frequency observations show periods of accretion and erosion and (not always correlated) widening and narrowing of the mudflat (Jaffe et al., in preparation).

## Model Setup

The model setup (Fig. 3, model input files at [Online Material](#)) describes a 1D, 1000 m long profile by 100 grid cells with  $dx = 10$  m. Numerical Courant conditions allow for a time step of 12 s. Inspired by the average 1858 profile, the initial bed level has an 800 m long, 3 m deep part adjacent to a 100-m channel slope and 100 m wide, 20 m deep channel. The Chézy defined roughness was kept constant at a value of  $65 \text{ m}^{1/2}/\text{s}$ . The bed linearly decays from 3- to 20-m depth between 800 and 900 m from the landward end. The deep channel area was added so that wave boundary conditions would not be affected by a limited water depth potentially developing during a morphodynamic model run.

The model is forced by a semi-diurnal tide with a 0.5-m water level amplitude at the channel end. Although the present mean tidal amplitude at Dumbarton Bridge is about 1 m (<http://tidesandcurrents.noaa.gov/stationhome.html?id=9414509&units=metric>), preliminary model results showed a closer match with measured profiles for a smaller tidal difference. The discussion section will address this.

Waves enter the domain from the channel end. We applied the ‘roller model’ option in 1D mode available in Delft3D to describe wave action across a profile (Deltare 2014, appendix B.15 and Roelvink et al. (2009) for a more advanced version

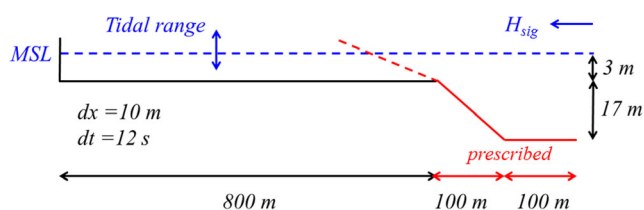


**Fig. 3** Model setup. Dotted red line indicates the channel slope prescription in case of accreting mudflat (colour figure online)

of the ‘roller’ approach). The roller model combines a wave action balance equation reflecting single frequency short waves to a roller energy equation representing infragravity waves originating from short wave dissipation via a breaker index formulation. At the lateral boundaries, it assumes zero gradients alongshore. Application of the roller model is possible in the case of a narrow-banded wave spectrum both with respect to frequency as with respect to direction. The main advantage of the roller model option is that it is faster than applying SWAN, since SWAN requires an extensive grid to prevent influence from the lateral boundaries and SWAN resolves time-consuming spectral short wave interactions. For example, runs for 100 years took about 3 h instead of 12 h using SWAN. Preliminary SWAN runs typically resulted in slightly steeper bed profiles for an equal wave height. We applied an online coupling of the roller wave model with Delft3D-FLOW so that both the effect of waves on current and the effect of flow on waves are accounted for. Still, effects of these interactions will be insignificant since preliminary model results show that modelled tidal flow velocities are typically an order of magnitude smaller than orbital velocities and short wave and roller energy propagation celerities. Also, at most locations, short wave energy appeared to be orders of magnitude larger than energy in the infragravity waves.

Mud transport is modelled by the well-known Krone-Partheniades formulation (Ariathurai 1974). Mud sediment concentration (Suspended Sediment Concentration, SSC) is prescribed at the channel boundary. A so-called “Thatcher-Harleman” condition at this boundary allows for a gradual 120-min relaxation from outgoing SSC levels to the prescribed SSC. This prevents sudden SCC variations at the turning of the tide.

In order to enhance bed level developments with respect to hydrodynamic forcing (Roelvink 2006), we used a morphological factor of 100. This approach is justified when bed level changes after a single time step do not fundamentally alter flow conditions above the bed. Although a strict criterion is hard to define, Roelvink (2006) suggests that bed level changes should not exceed 10 % of the water depth. A single hydrodynamic year thus covered hundred years of morphodynamic development. Sensitivity runs show very limited difference between such a run and a run of 100 years with a morphological factor of 1.

Sea level rise is included by prescribing a rise in mean sea level (MSL) at the channel boundary on top of the semi-diurnal forcing. We applied two SLR scenarios: a 1.67-m SLR/century close to the projected maximum SLR along the coast of California, while a 0.83-m SLR/century is closer to the projected mean SLR (NRC National Research Council 2012, Fig. 4).

Initial runs showed considerable deposition in the channel even to the extent of fully filling the channel. In reality, high along shore channel currents would prevent channel siltation.

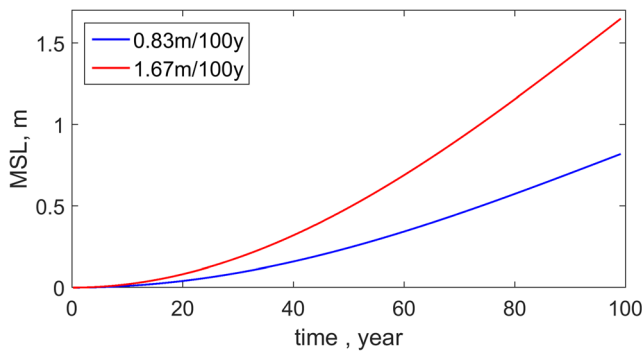


**Fig. 4** Imposed sea level rise (SLR)

To keep hydraulic boundary conditions constant during a run and for different sensitivity runs, the channel bed level (between 900 and 1000 m, horizontal red line in Fig. 3) was kept constant at a depth of 20 m by removing all deposited sediment after each time step, mimicking sediment erosion by along shore channel flow. In addition, preliminary model runs showed the development of a 3 grid cell wide and 0.3 m high spike at the mudflat edge. This was attributed to a numerical instability caused by high SSC, tidal flows over a very sharp bed level gradient. The instability was prevented by prescribing a gradual bed slope between 800 and 900 m which was about 1:5 for most of the channel slope and 1:20 for the last 20 m near the mudflat edge, allowing lower but not higher bed levels in this section. The 1:20 slope was maintained for sea level rise scenarios that included further mudflat accretion (dashed line in Fig. 3). The bed slope magnitude leading to stable results was determined iteratively. Comparison of runs with and without this correction showed similar mudflat profiles, implying that the prescription of the channel slope profile did not govern the level of the mudflat edge but only filtered the spike. To allow higher mudflat profiles under sea

level rise scenarios, we extrapolated the prescription of the channel slope (dotted red line in Fig. 3).

The first set of runs described 100 years of morphodynamic development starting from an initial mudflat level of 3 m below MSL. We carried out sensitivity analysis by varying a range of parameters one at a time (Table 1). We calibrated the model against the measured 2011 profile. Apart from sediment characteristics, the most important calibration parameter was the boundary condition wave height. Table 1 also presents observed values for the applied model parameters indicating sometimes large uncertainty bounds. The discussion section will address this.

A second set of runs started from an equilibrium mudflat profile generated in the first 100 years (by the “standard” run) and continued for another 100 years including the two SLR scenarios and scenarios of lower (22.5 mg/l) SSC at the channel boundary. This latter development is a plausible scenario given the major wetland restoration project in South Bay (Brew and Williams 2010, [www.southbayrestoration.org](http://www.southbayrestoration.org)). This project aims to restore about 6000 ha of industrial salt ponds to a rich mosaic of tidal wetlands and other habitats, attracting sediments and favouring sediment deposition in the salt ponds.

Model input files are provided as supplementary material. Software applied is open source Delft3D (<http://oss.deltares.nl/web/delft3d>).

## Model Results

### Equilibrium Profile

Model runs show slow development from a flatbed toward the 2011 measured profile within 50 years after which it hardly

**Table 1** Overview of model parameter variations in the sensitivity analysis

Parameter	Standard run	Minimum	Maximum	Observed
Tidal amplitude, $dH$ (m)	0.5	0.25	0.75	About 1 m ( <a href="http://tidesandcurrents.noaa.gov">http://tidesandcurrents.noaa.gov</a> )
Boundary SSC, $c$ (mg/l)	45	22.5	90	On average about 30 mg/l with monthly peaks between 100 and 300 mg/l and yearly peaks up to 1000 mg/l (Shellenbarger et al. 2013)
Initial mudflat depth, $dep_{ini}$ (m)	3	1	5	
Diffusion coefficient, $D$ ( $m^2/s$ )	10	1	20	
Significant wave height, $H_s$ (m)	0.123	0.09	0.15	On average about 0.25 m with occasional peaks of 1 m (Lacy et al. 2014 for a nearby mudflat)
Peak wave period $T_p$ (s)	2.5	2	3	
Erosion coefficient, $M$ ( $kg/m^2/s$ )	$5 \times 10^{-4}$	$5 \times 10^{-5}$	$5 \times 10^{-3}$	$1-5 \times 10^{-5}$ (in North Bay summarised by Van der Wegen et al. (2011))
Dry bed density, $\rho_{dry}$ ( $kg/m^3$ )	1200	1000	1600	
Critical erosion shear stress, $\tau_{cr,e}$ (Pa)	0.25	0.15	0.35	0.05–2 (in North Bay summarised by Van der Wegen et al. (2011))
Fall velocity, $w$ (mm/s)	1	0.1	2	0.1–10 (in North Bay summarised by Van der Wegen et al. (2011))
Morphological factor, MF (–)	100	25	200	

evolves anymore (see Fig. 5a and animation at [Online Material](#)). Initial deposition on the mudflat occurs near the channel edge after which the deposition front moves landward until it reaches the boundary. At the same time, deposition takes place at the channel side slope so that the mudflat further extends toward the channel. The mudflat extension continues until it reaches the prescribed channel slope between 800 and 1000 m. Any sediment depositing in the channel is removed to maintain the channel during the runs. The mudflat edge (near 760 m) remains lower than the prescribed (and allowed) bed level indicating that wave action limits mudflat accretion at this place. The bed level at the mudflat edge remains fairly constant during the remaining part of the model run, whereas the profile silts up slowly more landward.

Wave action alone does not lead to an intertidal mudflat (Fig. 5b). The small deposition at the mudflat in the absence of tides is the (limited) result of diffusive transport. Inclusion of tides only leads to significant deposition close to the channel, even to the extent that the remaining part of the mudflat is blocked. Larger waves lead to a lower mudflat. Variations of the erosion factor ( $M$ ) and critical erosion shear stress ( $\tau_{cr,e}$ ) applied in this study lead to similar profiles as the profiles by  $H_s$  variations shown in Fig. 5b. Higher SSC levels at the boundary lead to a higher and steeper mudflat profile, whereas the level of the mudflat edge interface remains fairly constant. The profiles by fall velocity variations lead to similar profile variations. Model results are not sensitive to the dry bed density and morphological factor variations, although a MF of 200 led to numerical instabilities after 60 years. A low diffusion coefficient shows less landward profile accretion, while

application of a higher diffusion shows hardly difference with the standard profile. Lower and higher initial mudflat depths lead to the same profile, albeit that the equilibrium profile is reached about 10 years earlier and later, respectively. A 2DV model with 10 vertical sigma layers leads to similar results. The profiles of low wave height and low boundary sediment concentration show a gap near the landward end indicating that they are not yet in equilibrium after 100 years.

The standard run shows a gradual decrease of the RMS error and development toward equilibrium after 50 years with a final RMS error of about 0.25 m (Fig. 6). Most other runs show similar behaviour, albeit with larger RMS errors. Two runs ( $w = 0.1$  mm/s and  $M = 5 \times 10^{-3}$  kg/m<sup>2</sup>/s) even show a smaller RMS error of about 0.15 m. Other runs show a minimum RMS error after some decades after which the error increases again. A fourth set of runs show only a gradual decrease of RMS error, which remains relatively large even after 100 years.

Closer analysis (Fig. 7) reveals that, initially, maximum SSC levels during a tidal cycle are lower than SSC levels at the boundary (45 mg/l). However, as the mudflat level becomes higher, maximum SSC levels increase up to values that are nearly double the SSC imposed at the boundary. These high SSC levels remain stable after about 75 years even when the bed level does hardly change anymore. Highest SSC levels of about 80 mg/l occur in the middle of the mudflat. For channel adjacent mudflats in a close-by San Francisco Bay sub-embayment, MacVean and Lacy (2014) also measured highest SSC in the intertidal area of the mudflat. MacVean and

**Fig. 5** **a** Modelled profile evolution. **b** Sensitivity analysis on profile after 100 years. The grey area reflects the observed tidal difference at Dumbarton Bridge

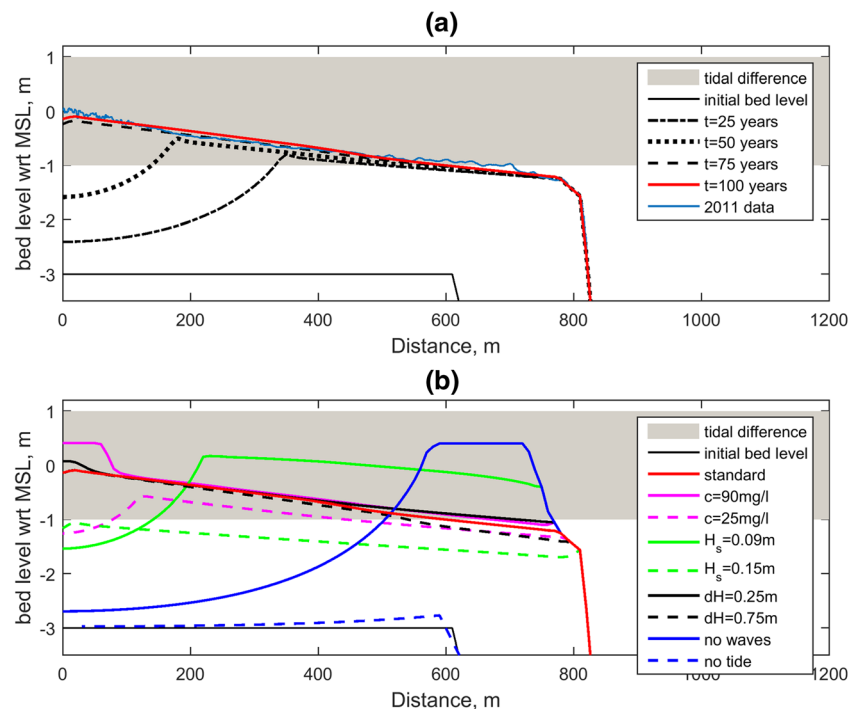
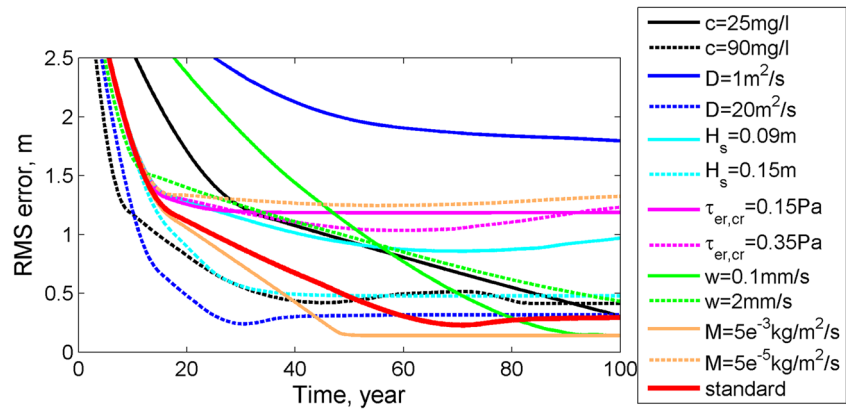


**Fig. 6** RMS error between measured and modelled bed profiles over time



Lacy (2014) report SSC levels during significant wave action in the range of 100–300 mg/l at subtidal stations, while SSC exceeded 1000 mg/l at the intertidal (more landward) station. More moderate wave conditions showed SSC levels comparable to our study. In addition, Brand et al. (2010) measured SSC level at two stations on a subtidal mudflat in South Bay. The SSC levels at the more landward located stations were about double the SSC at the deeper station close to the channel, while wave action tripled SSC for both stations.

Spikes of SSC occur between 40 and 70 years (Fig. 7a). These numerical instabilities develop first near the landward boundary when the deposition front just reaches the landward

boundary. They occur just after low water and persist for about an hour. Closer sensitivity analysis could not reveal the exact cause, but the instabilities seem to be related to wave breaking in cells close to the landward end (excluding the wave model does not lead to instabilities). The wave breaking results in sharp gradients in short wave and roller energy and (compared to the rest of the profile) relatively high roller energy levels at low water depth at the most landward point. These small instabilities are temporal (both during the tidal cycle and the morphodynamic evolution) and do not seem to disturb the general evolution trend.

The bed level does not develop gradually (Fig. 7b). In all three stations, the mud flat level initially linearly increases with time. When mudflat levels reach a certain level (lower levels for more landward locations), the accretion rate suddenly drops, because wave action limits (but does not block) accretion rates.

Starting at high water and during subsequent maximum ebb flow (hardly exceeding 0.5 mm/s), SSC levels remain relatively low although wave heights are high ( $t=0$ ,  $t=2$  h) (Fig. 8). When water depth on the mudflat further decreases and wave action starts to resuspend sediments from the mudflat, SSC levels significantly increase ( $t=4$  h,  $t=6$  h). Subsequent flood flow and larger water depth ( $t=8$  h) leads again to higher waves, while SSC levels drop when water depth becomes higher and wave impact decreases ( $t=10$  h). High SSC levels occur with a similar profile during both ebb and flood (compare conditions at  $t=4$  and  $t=8$ ), indicating that an equal amount of sediment is transported landward during flood and seaward during ebb.

Maximum shear stresses vary across the mudflat from 0.26 N/m<sup>2</sup> at the landward boundary during high water ( $t=0$  h) to 0.3 N/m<sup>2</sup> during low water ( $t=6$  h) (Fig. 9). Lowest shear stresses also vary considerably across the mudflat. Remarkably, shear stresses across the mudflat are lower than the critical erosion shear stress (0.25 N/m<sup>2</sup>) during a large part of the tidal cycle ( $t=0$ , 2 and 10 h). At high water ( $t=0$  h), only the shear stress close to the landward boundary exceeds the critical erosion shear stress. Tidally induced shear stresses are negligible compared to the contribution by wave action.

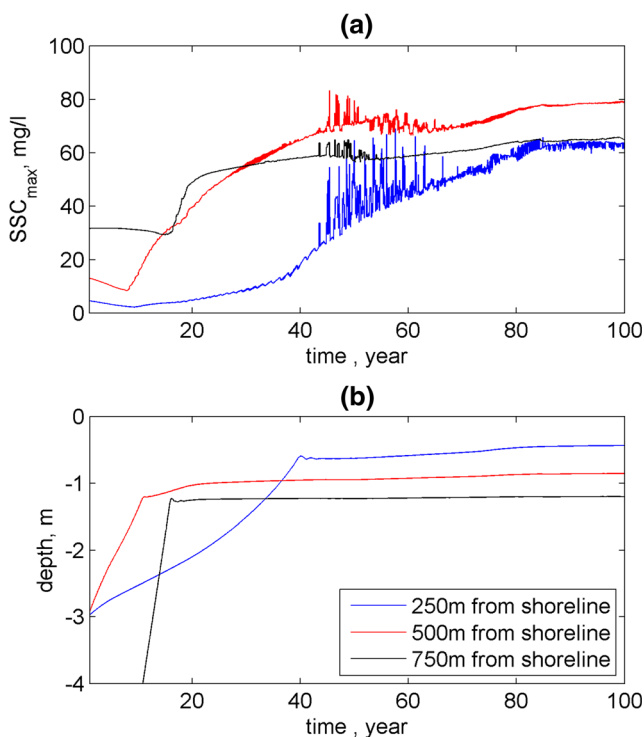


**Fig. 7** Evolution of tidally maximum SSC levels and bed levels across the mudflat

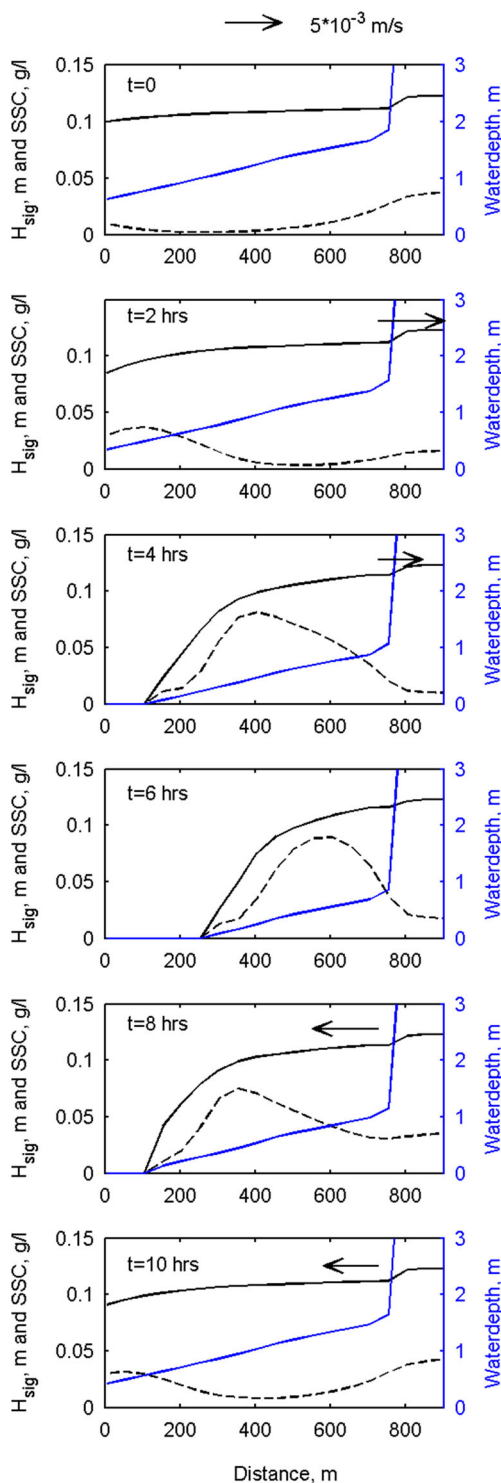


**Fig. 8** Hsig (black line), SSC (dashed black line) and water depth (blue line) during a tidal cycle along the standard mudflat profile after 50 years. Sequence starts at high water. Arrows denote tidal velocity at the channel slope (colour figure online)

A possible explanation of the modelled mudflat accretion and the developing equilibrium conditions is as follows. On a deep mudflat bed, mud initially deposits close to the mudflat edge. As this area becomes shallower, wave action resuspends

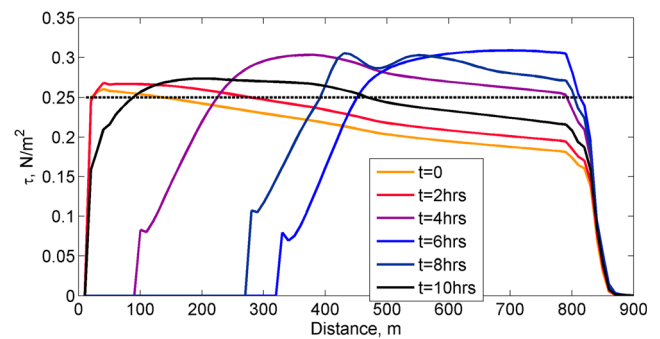


**Fig. 9** Shear stress during a tidal cycle along the standard mudflat profile after 50 years. High water slack is at  $t=0$ . Dotted black line indicates critical erosion shear stress,  $\tau_{ce}$

the sediments during low water. Subsequent flood flow transports this mud landward where it deposits. Wave action during ebb flow is not able to resuspend these sediments so that the mudflat also accretes and a depositional front migrates landward. This process continues until the mudflat profile reaches equilibrium conditions when the sediment that is transported landward during flood is resuspended and transported seaward during ebb. This implies that tide residual sediment transport and its spatial gradients across the mudflat are (almost) not present after 50 years. During equilibrium conditions, the shear stress at the landward boundary hardly exceeds the critical shear stress for erosion indicating that, from that location, no sediment can be transported seaward during subsequent ebb flows.

### Sea Level Rise

Starting from the 100-year mudflat profile generated by the standard run, we performed 100-year runs imposing scenarios of SLR and lower SSC levels at the boundary. SLR leads to a proportionally higher mudflat profile which is similar in shape to the standard run, albeit with a slightly gentler slope (solid lines in Fig. 10a and in the animation at [Online Material](#)). The mudflat becomes narrower as the mudflat edge develops along the imposed bed level slope (Fig. 3). Doubling SLR (from 0.83 to 1.67 m/century) roughly leads to a doubling of mudflat accretion (0.6 m to about 1.2 m/century). An abrupt 50 % reduction in SSC level at the boundary leads to an almost uniformly lower mudflat profile of about 0.15 m, although the mudflat erosion remains limited at the landward end (Fig. 10b). Combination of lower SSC and both SLR scenarios leads to lower profiles as well similar to the standard case. Exceptionally, a combination of high SLR (1.67 m/century) and a drop in SSC level lead to a mudflat that does not accrete anymore at the landward end.

There are two adaptation timescales (Fig. 10b). An abrupt 50 % decay of SSC has a relatively fast effect on the mean mudflat level (a decrease of about 0.15 m within 20 years for a

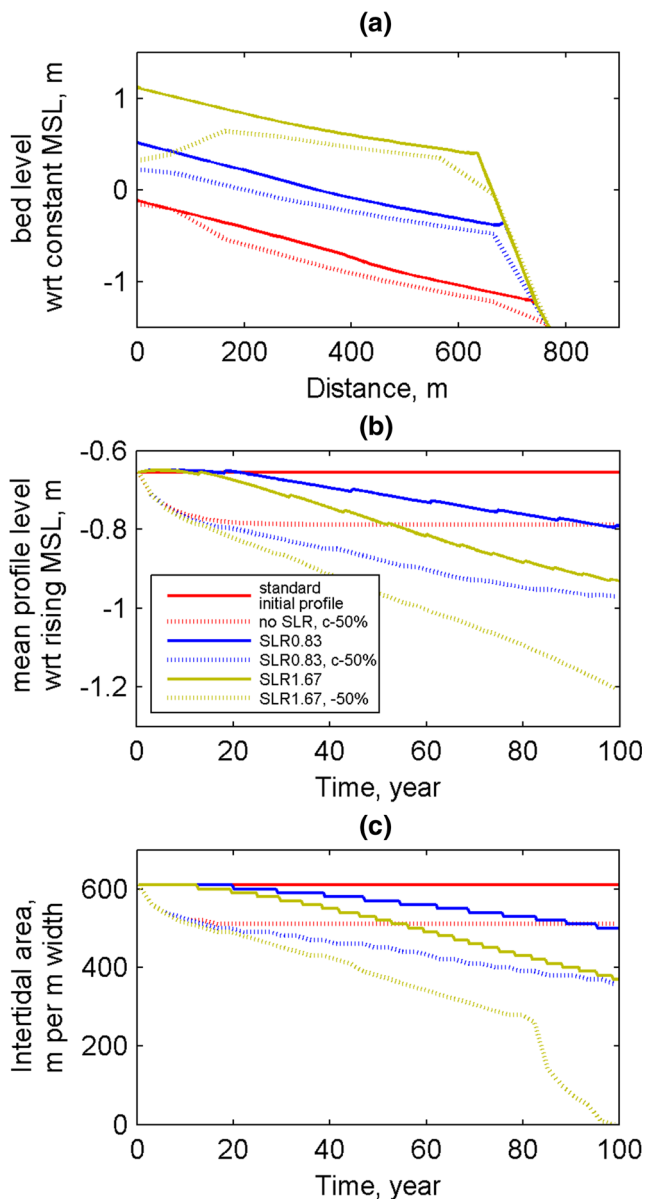


**Fig. 10** **a** Profiles by SLR and SSC scenarios after 100 years with respect to constant MSL. Profile evolution under different scenarios: **b** mean mudflat depth and **c** meter intertidal area. The observed tidal range is 1 m. The applied tidal range in the model results is 0.5 m and is constant for the sea level rise scenarios

constant MSL), which stabilise afterward (dotted red line). SLR drowns the mudflat more slowly, albeit at a continuous rate (about 0.27 m over 100 years for the 1.67-m SLR scenario). Although the mudflat accretes under SLR scenarios, it also drowns because of the larger increase in MSL. This is apart from the effect of the shortening of the mudflat due to the imposed channel slope. Figure 10c shows that intertidal area decreases as well. A higher SLR leads to faster loss of intertidal area. Of the original amount of intertidal area, about 65 % remains after 100 years under a SLR scenario of 1.67 m/century. The sudden drop in the scenario of 1.67 m/century sea level rise in combination with a 50 % SSC decrease is

explained by the limited accretion at the landward end (see Fig. 10a). Although the mudflat length decreased due to the imposed extrapolation of the channel slope, the intertidal portion of the mudflat remained always 600 m or less, i.e. less than the minimum mudflat length of about 620 m so that mudflat length decrease did not contribute to intertidal area decrease. The amount of intertidal area was calculated with a tidal amplitude of 1 m, which is the mean tidal amplitude measured at Dumbarton mudflat.

The mudflat accretes under SLR scenarios. The gentler mudflat slope under SLR scenarios suggests that the mudflat adapts by a (very small) deposition front gradually moving from the mudflat edge toward the landward end, similar to the mudflat evolution in Fig. 5a. This process explains the gap near the landward end in the 1.67 m/century SLR and 50 % SSC drop scenario. At a certain moment, SLR leads to a water depth at which waves cannot resuspend sediments at the deposition front anymore at low water. At that moment, landward front migration comes to a halt. Additional runs (not shown) indicate that the same gap develops for higher SLR scenarios and longer mudflats under equal SLR scenarios (both without SSC decrease).

## Discussion

### Model Schematisation

Our modelling exercise satisfactorily reproduces an observed mudflat profile applying physically reasonable input parameters. This is despite considerable simplifications concerning plan form and forcing.

An example of a simplification covering probably more complex dynamics is the applied tidal amplitude of 0.5 m. This is smaller than the average tidal amplitude of 1 m and also neglects more complex tidal oscillations with diurnal constituents present in the Dumbarton mudflat area. Still, the 0.5-m amplitude leads to better decadal timescale results, while a higher (lower) value leads to a steeper (gentler) profile (see Fig. 5b), suggesting that conditions smaller than the observed tidal amplitude govern morphodynamic development. Another explanation is that processes not considered in this study (such as along mudflat currents or mud particle gradation) could make the mudflat slope more gentle while maintaining the observed tidal amplitude.

Another major assumption is the imposed bed profile of the channel slope not only between 700 and 1000 m but also at higher mudflat profiles. This leads to a narrower mudflat in case the mudflat accretes such under SLR scenarios (Fig. 3). Morphodynamic processes at the channel slope are difficult to include following our 1D approach. Preliminary model tests imposing an along shore current in the channel reach and on the mudflat by means of a water level gradient across the

lateral boundary (i.e. Neumann boundaries) lead to unstable model results. Gong et al. (2009) present a more successful (although still not fully stable) 2D modelling effort applying Neumann boundary conditions on a mud coast model with a largely subaqueous mudflat. Van der Wegen et al. (2011), Van der Wegen and Jaffe (2013) and Van der Wegen and Jaffe (2014) present a skillful 2D modelling effort on hindcasting and analysing decadal timescale morphodynamics in North San Francisco Bay. The channel shoal interface is similar to the Dumbarton mudflat conditions although the plan form with rocky outcrops had a governing impact on the developing morphodynamics in San Pablo Bay.

A major simplification concerns the 1D approach. Our study applies a profile model where waves and tide enter from the channel toward the shore. However, prevailing conditions at Dumbarton mudflat are different. Tides propagate from north to south along the mudflat. Persistent northerly to north-westerly winds occur during the summer, while gusty, southerly to south-easterly winds prevail during the winter. These winds will generate waves propagating along rather than across the mudflat. In addition, the mudflat width is not uniform along the channel while the adjacent bridge at the northern boundary may have significant impact by the bridge piers inducing turbulence patterns. Along-shore currents may play an important role enhancing shear stresses and sediment resuspension at the mudflat. Brand et al. (2010) and Lacy et al. (2014) observed currents of up to 0.3 m/s at nearby San Francisco Bay mudflats. Not considering wave current interactions, these currents lead to a shear stress of approximately  $0.21 \text{ N/m}^2$ , which is similar to the modelled wave-induced shear stress (Fig. 9). This suggests that our model underestimates the importance of tidal flows relative to wave action.

A number of reasons may explain why the model still reproduces the measured profile so well. Wave height at the mudflat is depth limited and a correct wave direction seems of less importance. The value of the wave model is to provide an extra bed shear stress in addition to the relatively low tidal currents. The modelled waves could thus reflect waves coming from any direction. The modelled tidal currents are low and are important to transport wave resuspended sediments onto the mudflat. Along-shore tidal currents at the mudflat entering and leaving the model from its lateral (northern and southern) boundaries may do the same. Assuming uniform tidal conditions along the mudflat, these boundaries will probably supply and take along a similar amount of sediment not leading to a significant (first order) net morphodynamic effect. On the other hand, conditions at Dumbarton mudflat are not constant with bridge piers intersecting the mudflat at the northern boundary and a wider mudflat at the southern boundary. Future research may explore 2D effects and dynamics in more detail.

## Equilibrium

The modelled profile is in morphodynamic equilibrium. Although sediment resuspension and deposition (and associated small (~mm) bed level changes) occur during a tidal cycle, the tide residual transports remain negligible. Confirming model results by Roberts et al. (2000) and measurements by MacVean and Lacy (2014) and Brand et al. (2010), the equilibrium profile allows for high SCC levels during a tidal cycle. A profile maintaining uniform and equal to or lower than critical erosion shear stress across the mudflat profile is not needed for equilibrium conditions. Such a profile would thus reflect a limit deeper than the equilibrium profile obtained in this study.

Although model results could reproduce the 2011 measured profile quite well, it may be questioned whether the modelled equilibrium conditions reflect an actual equilibrium state of the measured profile as well. Just as argued in the discussion on SSC and SLR induced adaptation time scales, the measured mudflat profile may be, and probably is, in an adaptation process due to past changes in forcing. Historic developments were considerable, but more recent bathymetries indicate much less morphodynamic activity (Fig. 2). If we assume that currently on-going morphodynamic developments associated with past changes in forcing will remain small compared to the SSC and SLR scenarios, the equilibrium conditions obtained by the standard run offer an excellent opportunity to start systematically exploring the impact of changing boundary conditions such as SLR and SSC variations.

Still, this equilibrium condition raises a number of questions. In reality, forcing conditions will not be constant. Tides, wind, wind waves and associated sediment transport vary on a daily to seasonal timescale. Sediment characteristics (varying grain size, critical shear stress, erosion factor or fall velocity) may vary seasonally as well, for example due to the presence of biofilms, consolidation or varying supply of organic matter stimulating flocculation processes (e.g. Zhou et al. 2016; Widdows et al. 2000; Friedrichs 2012). Shellenbarger et al. (2013) shows the seasonal variation in SSC at the Dumbarton Bridge site. Furthermore, extreme wind and wave events may temporally adjust the profile and could, for example, play an important role in filling the gap developing at the landward end on high SLR scenario (see Fig. 10a).

We stress that our approach applies considerable time averaging of forcing conditions. The forcing conditions and sediment characteristics defined in the current model must thus be considered as accounting for or neglecting of variations on a time scale smaller than modelled characteristic developments. It is possible that that daily to yearly variations simply do not have an effect on decadal time scale mudflat evolution. It is also possible that the effect of daily to yearly variations is somehow included in the model calibration parameters. The

model will thus not capture the effect of individual extreme events, but rather considers their average effect in the calibration parameters. For example, individual events with high waves, strong wind-induced currents (or even along-shore currents) may be represented in the model by an increased mean wave height. This approach is possible when the mudflat system is resilient. Extreme events should not fundamentally change the mudflat system so that regular and prevailing conditions can recover the impact by extreme events and the system can be modelled by average forcing.

### Impact of Sea Level Rise

The mudflats under SLR scenarios are not in equilibrium. Adaptation time scales as the result of abruptly changing boundary conditions (e.g. drop in SSC) may be decades. In the SLR scenarios, mudflats are still adapting, while boundary forcing even continues to change as well. As shown in Fig. 5a, the mudflat builds up from channel to the landward end. The gentler profiles under SLR scenarios are thus probably the result of relatively more accretion at the mudflat edge than at the landward end. A SCC decrease leads to a contrasting process, where more sediment erodes near the landward end than at the mudflat edge, leading to a gentler profile as well (Fig. 10a). Along this line of thought, if SLR would abruptly stop, the mudflats will continue to adapt leading to a steeper and shallower profile similar to but higher than the standard profile.

Model results suggest that changing boundary conditions may not only drown mudflats but can also make them less stable. This is due to the character of the mudflat adaptation process with bed levels near the channel adapting faster than the bed level near the landward end. When SLR is too large, the mudflat is too long or SSC levels drop too fast; the landward-directed mudflat growth comes to a halt creating depressions between the maximum mudflat level at the depositional front and the landward end. Tidal flows directed along a mudflat could easily further excavate these depressions into ebb drainage and flooding channels. Figure 2 shows the historic presence of such a channel at Dumbarton Bridge mudflat.

### Ecological Values

Sea level rise is a potential threat to many estuarine, intertidal mudflats. This holds in particular for engineered systems in which the landward end of the mudflat is bounded by levees protecting hinterland against flooding. Although the mudflat will continue to exist, intertidal area will disappear. In such scenarios, ecological values associated with intertidal mudflats (such as feeding ground for birds) will be put under pressure. Action is required to maintain ecological functions, for example, by allowing landward migration through landward levee replacement. This research suggests that intertidal will disappear under all sea level rise scenarios, but those developments

are quite gradual. This implies that there is time and opportunity to develop adaptation strategies in policy making.

### Conclusions

Measured mudflat profiles over the past 150 years on Dumbarton mudflat show that considerable profile development occurred as the result of changing sediment supply.

Our 1D modelling effort reproduces the current mudflat profile in an equilibrium condition that maintains high SSC levels. An important indicator for reaching equilibrium conditions is that shear stresses are not exceeding the critical threshold for erosion during high water, while the highest shear stress under high water conditions is at the landward end.

Probably, our approach is possible due to the system's resilience. This implies that extreme events should not be able to fundamentally change the mudflat system so that regular and prevailing conditions can recover the impact by extreme events and the system can be modelled by average forcing.

Model results suggest that the mudflat will lose a considerable amount of intertidal area when suggested SLR and SSC scenarios will occur. Also, mudflats may become more unstable since the landward accumulation comes to a halt when mudflats are too long, SLR is too high or SSC decrease is too fast. Under these conditions, channel development may occur at landward locations that could not adapt fast enough to the changing conditions.

Future research may explore the impact of grain sorting, extreme wind/wave events, 2D configurations accounting for along mudflat tidal flows and wave action and morphodynamic processes at the channel-shoal interface.

**Acknowledgments** This work was financially supported by the California Landscape Conservation Cooperative (CA LCC). We highly appreciated the constructive comments by the associate Editor, Marianne Holmer, and two anonymous reviewers. Jessica Lacy (USGS) provide valuable feedback on a preliminary version of this work, while Pieter Koen Tonnon, Mart Bosboom and Bert Jagers (Deltares) assisted in the numerical methodology and wave module application.

**Open Access** This article is distributed under the terms of the Creative Commons Attribution 4.0 International License (<http://creativecommons.org/licenses/by/4.0/>), which permits unrestricted use, distribution, and reproduction in any medium, provided you give appropriate credit to the original author(s) and the source, provide a link to the Creative Commons license, and indicate if changes were made.

### References

- Ariathurai, C.R. 1974. *A finite element model for sediment transport in estuaries*, Ph.D. thesis. Davis: Univ. of Calif. Davis.

- Barnard, P.L., D.H. Schoellhamer, B.E. Jaffe, and L.J. McKee. 2013. *Sediment transport in the San Francisco Bay coastal system: an overview*. Marine Geology: 345.
- Bearman, J.A., C.T. Friedrichs†, B.E. Jaffe, and A.C. Foxgrover. 2010. Spatial trends in tidal flat shape and associated environmental parameters in South San Francisco Bay. *Journal of Coastal Research* 26: 2: 342–349.
- Brand, A., J.R. Lacy, K. Hsu, D. Hoover, S. Gladding, and M.T. Stacey. 2010. Wind-enhanced resuspension in the shallow waters of South San Francisco Bay: mechanisms and potential implications for cohesive sediment transport. *J. Geophys. Res.* 115: C11024. doi:10.1029/2010JC006172.
- Brew, D.S., and P.B. Williams. 2010. Predicting the impact of large-scale tidal wetland restoration on morphodynamics and habitat evolution in south San Francisco Bay, California. *Journal of Coastal Research* 26:5: 912–924. doi:10.2112/08-1174.1.
- Cheng, R.T., V. Casulli, and J.W. Gartner. 1993. Tidal, residual, intertidal mudflat (TRIM) model and its applications to San Francisco Bay, California. *Estuarine, Coastal and Shelf Science* 36(3): 235–280.
- Conomos, T.J., and D.H. Peterson. 1977. Estuarine processes. In *Suspended particle transport and circulation in San Francisco Bay: an overview*, ed. M. Wiley. Academic, 82–97.
- Conomos, T.J., R.E. Smith, and J.W. Gartner. 1985. Environmental setting of San Francisco Bay. *Hydrobiologia* 129(1): 1–12.
- Deltares. 2014. *Delft3D Flow User Manual*. Available at <http://oss.deltares.nl/web/delft3d/manuals>.
- Foxgrover, A.C., S.A. Higgins, M.K. Ingraca, B.E. Jaffe, and R.E. Smith. 2004. *Deposition, erosion, and bathymetric change in South San Francisco Bay: 1858–1983*. U.S. Geological Survey Open-File Report 2004–1192, 25. <http://pubs.usgs.gov/of/2004/1192>.
- Friedrichs, C.T. 2012. Tidal flat morphodynamics: a synthesis. In *Treatise on Estuarine and Coastal Science*, vol. 3, ed. J.D. Hanson and B.W. Flemming, 137–170. Estuarine and Coastal Geology and Geomorphology.
- Friedrichs, C.T., and D.G. Aubrey. 1996. Uniform bottom shear stress and equilibrium hypsometry of intertidal flats. In *Mixing in Estuaries and Coastal Seas, Coastal and Estuarine Stud.* 50, ed. C. Pattiaratchi, 405–429. Washington: AGU.
- Ganju, N.K., and D.H. Schoellhamer. 2010. Decadal-timescale estuarine geomorphic change under future scenarios of climate and sediment supply. *Est. and Coasts* 33: 15–29. doi:10.1007/s12237-009-9244-y.
- Ganju, N.K., D.H. Schoellhamer, and B.E. Jaffe. 2009. Hindcasting of decadal-timescale estuarine bathymetric change with a tidal-timescale model. *J. Geophys. Res.* 114: F04019. doi:10.1029/2008JF001191.
- Ganju, N.K., M.L. Kirwan, P.J. Dickhudt, G.R. Guntenspergen, D.R. Cahoon, and K.D. Kroeger. 2015. Sediment transport-based metrics of wetland stability. *Geophys. Res. Lett.* 42. doi:10.1002/2015GL065980.
- Gong, Z., Z. Wang, M.J.F. Stive, C. Zhang, and A. Chu. 2009. Process-Based Morphodynamic Modeling of a Schematized Mudflat Dominated by a Long-Shore Tidal Current at the Central Jiangsu Coast, China. *J. of Coast. Res.* 28(6): 1381–1392.
- Herman, P.M.J., J.J. Middelburg, J. van de Koppel, and C.H.R. Heip. 1999. Ecology of estuarine macrobenthos. *Advances in Ecology Research* 29: 195–240.
- Hsu, Tian-Jian, Chen Shih-Nan, and Andrea S. Ogston. 2013. The landward and seaward mechanisms of fine-sediment transport across intertidal flats in the shallow-water region - a numerical investigation. *Continental Shelf Research* 60. doi:10.1016/j.csr.2012.02.003.
- Hu, Z., Z.B. Wang, T.J. Zitman, M.J.F. Stive, and T.J. Bouma. 2015. Predicting long-term and short-term tidal flat morphodynamics using dynamic equilibrium theory. *J. Geophys. Res. Earth Surf.* 120. doi:10.1002/2015JF003486.
- Jaffe, B., and A. Foxgrover. 2006. *A history of intertidal flat area in south San Francisco Bay, California; 1858 to 2005*. Open-File Report — U. S. Geological Survey.
- Jones, C.A., and B.E. Jaffe. 2013. Influence of history and environment on the sediment dynamics of intertidal flats. *Marine Geology* 345: 294–303. doi:10.1016/j.margeo.2013.05.011.
- Lacy, J.R., D.H. Schoellhamer, and J.R. Burau. 1996. Suspended-solids flux at a shallow-water site in South San Francisco Bay, California. In *North American Water and Environment Congress & Destructive Water*, 3357–3362. ASCE.
- Lacy, J.R., S. Gladding, A. Brand, A. Collignon, and M.T. Stacey. 2014. Lateral baroclinic forcing enhances sediment transport from shallows to channel in an estuary. *Estuaries and Coasts*. doi:10.1007/s12237-013-9748-3.
- Le Hir, P., W. Roberts, O. Cazaillet, M. Christie, P. Bassoullet, and C. Bacher. 2000. Characterization of tidal flat hydrodynamics. *Continental Shelf Research* 20: 433–459.
- Maan, D.C., B.C. Prooijen, Z.B. Wang, and H.J. De Vriend. 2015. Do Intertidal Flats Ever Reach Equilibrium? *Journal of Geophysical Research Earth Surface* doi. doi:10.1002/2014JF003311.
- MacVean, L.J., and J.R. Lacy. 2014. Interactions between waves, sediment, and turbulence on a shallow estuarine mudflat. *J. Geophys. Res. Oceans* 119: 1534–1553. doi:10.1002/2013JC009477.
- Marani, M., A. D'Alpaos, S. Lanzoni, L. Carniello, and A. Rinaldo. 2007. Biologically controlled multiple equilibria of tidal landforms and the fate of the Venice lagoon. *Geophys. Res. Lett.* 34: L11402. doi:10.1029/2007GL030178.
- Mariotti, G., and S. Fagherazzi. 2010. A numerical model for the coupled long term evolution of salt marshes and tidal flats. *J. Geophys. Res.* 115: F01004. doi:10.1029/2009JF001326.
- Möller, I., M. Kudella, F. Rupprecht, T. Spencer, M. Paul, B.K. van Wesenbeeck, and S. Schimmels. 2014. Wave attenuation over coastal salt marshes under storm surge conditions. *Nature Geoscience* 7: 727–731. doi:10.1038/ngeo2251.
- NRC (National Research Council). 2012. *Sea-level rise for the Coasts of California, Oregon, and Washington: past, present, and future*. Washington: National Academic Press.
- Pritchard, D., and A.J. Hogg. 2003. Cross-shore sediment transport and the equilibrium morphology of mudflats under tidal currents. *Journal of Geophysical Research* 108(C10): 3313. doi:10.1029/2002JC001570.
- Pritchard, D., A.J. Hogg, and W. Roberts. 2002. Morphological modelling of intertidal mudflats: the role of cross-shore tidal currents. *Continental Shelf Research* 22(11–13): 1887–1895. doi:10.1016/S0278-4343(02)00044-4.
- Roberts, W., P. Le Hir, and R.J.S. Whitehouse. 2000. Investigation using simple mathematical models of the effect of tidal currents and waves on the profile shape of intertidal mudflats. *Continental Shelf Research* 20: 1079–1097.
- Roelvink, J.A. 2006. Coastal morphodynamic evolution techniques. *Journal of Coastal Engineering* 53: 177–187.
- Roelvink, J.A., A. Reniers, A.P. van Dongeren, J.V.T. de Vries, R. McCall, and J. Lescinski. 2009. Modelling storm impacts on beaches, dunes and barrier islands. *Coastal engineering* 56(11): 1133–1152.
- Schoellhamer, D.H. 1996. Factors affecting suspended-solids concentrations in South San Francisco Bay, California. *Journal of Geophysical Research: Oceans* 101(C5): 12087–12095.
- Shellenbarger, Gregory G., Scott A. Wright, and David H. Schoellhamer. 2013. A sediment budget for the southern reach in San Francisco Bay, CA: implications for habitat restoration. *Marine Geology* 345: 281–293. doi:10.1016/j.margeo.2013.05.007.
- Temmerman, S., G. Govers, S. Wartel, and P. Meire. 2004. Modelling estuarine variations in tidal marsh sedimentation: response to changing sea level and suspended sediment concentrations. *Marine Geology* 212(1): 1–19.

- Van der Wegen, M., and B.E. Jaffe. 2014. Processes governing decadal-scale depositional narrowing of the major tidal channel in San Pablo Bay, California, USA. *J. Geophys. Res. Earth Surf* 119. doi:[10.1002/2013JF002824](https://doi.org/10.1002/2013JF002824).
- Van der Wegen, M., and B.E. Jaffe. 2013. Towards a probabilistic assessment of process-based, morphodynamic models. *Coastal Engineering* 75: 52–63. doi:[10.1016/j.coastaleng.2013.01.009](https://doi.org/10.1016/j.coastaleng.2013.01.009).
- Van der Wegen, M., B.E. Jaffe, and J.A. Roelvink. 2011. Process-based, morphodynamic hindcast of decadal deposition patterns in San Pablo Bay, California, 1856–1887. *J. Geophys. Res.* 116: F02008. doi:[10.1029/2009JF001614](https://doi.org/10.1029/2009JF001614).
- Van Maren, D.S., and J.C. Winterwerp. 2013. The role of flow asymmetry and mud properties on tidal flat sedimentation. *Continental Shelf Research* 60(S): 71–84.
- van Wijnen, H.J., and J.P. Bakker. 2001. Long-term surface elevation change in salt marshes: a prediction of marsh response to future sea-level rise. *Estuarine Coastal and Shelf Science* 52: 381–390.
- Walters, R.A., R.T. Cheng, and T.J. Conomos. 1985. Time scales of circulation and mixing processes of San Francisco Bay waters. *Hydrobiologia* 129: 13–36.
- Widdows, J., S. Brown, M.D. Brinsley, P.N. Salkeld, and M. Elliott. 2000. Temporal changes in intertidal sediment erodability: influence of biological and climatic factors. *Continental Shelf Res.* 20: 1275–1289.
- Zhou, Z., G. Coco, M. van der Wegen, Z. Gong, Ck Zhang, and I. Townend. 2015a. Modeling sorting dynamics of cohesive and non-cohesive sediments on intertidal flats under the effect of tides and wind waves. *Continental Shelf Research* 104: 76–91. doi:[10.1016/j.csr.2015.05.010](https://doi.org/10.1016/j.csr.2015.05.010).
- Zhou, Z., Qinghua Ye, and Giovanni Coco. 2015b. A one-dimensional biomorphodynamic model of tidal flats: sediment sorting, marsh distribution, and carbon accumulation under sea level rise. *Advances in Water Resources*. doi:[10.1016/j.advwatres.2015.10.011](https://doi.org/10.1016/j.advwatres.2015.10.011).
- Zhou, Z., Mick van der Wegen, Jagers Bert, and Coco Giovanni. 2016. Modelling the role of self-weight consolidation on the morphodynamics of accretional mudflats. *Environmental Modelling & Software* 76: 167–181. doi:[10.1016/j.envsoft.2015.11.002](https://doi.org/10.1016/j.envsoft.2015.11.002).